JOURNAL OF GEOPHYSICAL RESEARCH, VOL. 102, NO. B9, PAGES 20,211–20,224, SEPTEMBER 10, 1997

Effect of crystal defects and internal stress on the domain structure and magnetic properties of magnetite

Özden Özdemir and David J. Dunlop

Department of Physics, Erindale College, University of Toronto, Mississauga, Ontario, Canada

Abstract. Domain structures in magnetite are very sensitive to crystal imperfections, which play a major role in hysteresis and remanence by hindering the motion of domain walls. Using the Bitter colloid technique, we have observed spike and closure domains of the style predicted by *Néel* [1944] around nonmagnetic inclusions, chemically altered regions, and grain boundaries in a natural single crystal of magnetite. Isolated inclusions within body domains have pairs of attached Néel spikes which reduce magnetostatic energy by diluting magnetic poles. In one example we calculated that spikes reduced the energy by a factor of 6-7. In some cases 71°, 109° and 180° domain walls are pinned to defects either through spikes or via chains of subsidiary closure domains. One example of pinning by a spike gave a calculated microcoercivity of 0.54 mT, similar to the bulk coercive force of 0.5 mT for the crystal. "Colloid gaps" in 180° and other walls form lines parallel to a <111> easy axis and are evidence of underlying line defects, for example, dislocations, whose stress fields deflect the spins locally, weakening the magnetic field gradient above the walls. We have also observed bending of 180° walls anchored at pinning sites on the grain boundary, the first direct experimental evidence of the effect of internal stresses on the domain structure of magnetite. We determined internal stress magnitudes in the range 7- 34 MPa from the observed linear dimension and transverse displacement of each bowed wall. Finally, we measured hysteresis curves on a companion magnetite crystal at temperatures T from ambient to the Curie point of 585°C. Observed coercivity H_c varies with T as $\lambda_{111}w^{0.5}/M_s$, in agreement with theoretical predictions of impedance of a wall of width w by dislocation stress fields. We therefore propose that the stability of remanence in multidomain magnetite is mainly due to pinning of domain walls by crystal defects.

Introduction

Paleomagnetic records of plate motions exist because magnetic minerals remember past geomagnetic fields through their remanent magnetization or remanence. How well the remanence has resisted later changes in the field cannot be measured directly, but a useful indicator is coercivity, measured by alternating field (AF) demagnetization or hysteresis (coercive force H_c; remanent coercive force H_{cr}).

Titanomagnetite with a composition near magnetite (Fe_3O_4) carries much of the remanence of continental and oceanic rocks and sediments. Ultrafine magnetite crystals with diameters ≤0.1 μm (or somewhat larger if elongated) are magnetically homogeneous. Such single-domain (SD) crystals have strong, stable remanence because the magnetic lattice must be rotated against anisotropy forces. In nature, however, SD magnetite is confined to volcanic glasses, magnetic bacteria and their fossils, and needle-like inclusions in magmatic silicates.

Practically all other natural magnetite crystals are magnetically inhomogeneous, containing domains of uniform spontaneous magnetization $\mathbf{M}_s$ separated by narrow walls in which atomic spins rotate smoothly. Walls are generally planar (Figure 1) and bisect the angle between $\mathbf{M}_s$ vectors in the adjacent domains in order to avoid magnetic poles (surface density $\mathbf{M}_s \cdot \hat{\mathbf{n}}$, where $\hat{\mathbf{n}}$ is the normal to the boundary, in this case the wall) which would increase the magnetostatic energy E_m.

Domains and walls with the same basic character shown in Figure 1, or with subsidiary flux closure domains, have been imaged over a very broad size range in magnetite, extending from 0.5-1 μm (Lorentz microscopy [*Smith*, 1980]; Bitter colloid patterns [*Geiß et al.*, 1996]) to tens or hundreds of μm (magneto-optical Kerr effect [*Worm et al.*, 1991; *Heider and Hoffmann*, 1992], magnetic force microscopy [*Williams et al.*, 1992; *Proksch et al.*, 1994; *Pokhil and Moskowitz*, 1996], Bitter patterns [*Özdemir and Dunlop*, 1993; *Özdemir et al.*, 1995]). Crystals smaller than 0.5-1 μm but larger than SD size are also predicted to have recognizable domains and walls or wall-like vortex structures as one of their micromagnetic states [*Williams and Dunlop*, 1990; *Newell et al.*, 1993; *Fabian et al.*, 1996]. Our observations in the present paper are therefore likely to have broad relevance to small as well as large multidomain (MD) grains.

In a defect-free MD crystal, wall motion is easy. If a field $\mathbf{H}_0$ is applied parallel to 180° domain walls (Figure 1), the walls will be displaced reversibly so as to enlarge domains with $\mathbf{M}_s$ parallel to $\mathbf{H}_0$, returning to zero remanence positions when $\mathbf{H}_0 \rightarrow 0$. The remanence and coercivity are both zero; there is no hysteresis. However, real crystals have defects of one kind or another. Wall displacements are impeded by these defects, and the walls remain pinned away from their original positions. This is the main source of coercivity, remanence, and hysteresis in MD crystals.

In addition to irreversible wall motion involving defect pinning, hysteresis is affected by wall nucleation. However, nucleation will

Paper number 97JB01779.
0148-0227/97/97JB-01779$09.00

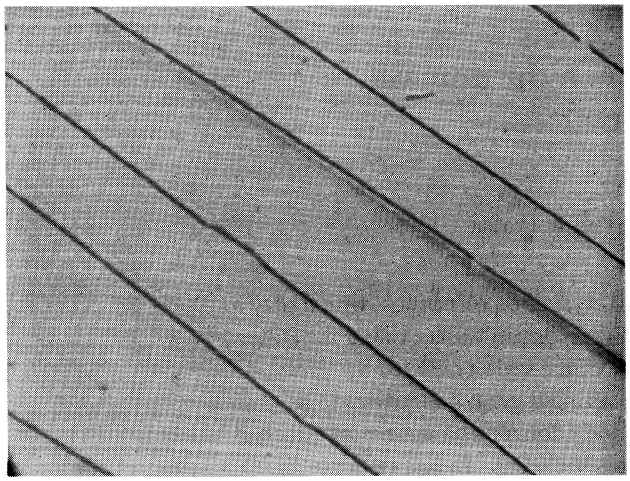

Figure 1. Simple 180° domain walls on a strain-free {110} viewing plane (triangle ABC in Figure 2) of a 3 mm natural single crystal of magnetite.

not by itself produce remanence because the internal demagnetizing field will minimize the demagnetizing energy E_m by moving all walls, including newly nucleated walls, to positions where the domain magnetizations are mutually cancelling. Pinning of walls in out-of-equilibrium positions is still required to produce remanence.

The kinds of defects that can pin walls include volume defects like voids and nonmagnetic inclusions, line and planar defects like dislocations and stacking faults, and irregularities on boundaries such as cracks, regions of alteration, or grain surfaces. Walls cling to inclusions or voids: to large ones because they have attached subsidiary domains (e.g., Néel spikes [*Néel*, 1944]), which form to dilute magnetic poles on the void and reduce E_m; and to small ones because they reduce the volume of any walls that contain them, thereby reducing the wall energy E_w [*Kersten*, 1943; *Dijkstra and Wert*, 1950].

Stacking faults are common planar defects in magnetite [*Jakubovics et al.*, 1978; *Banfield et al.*, 1994]. The commonest line defects are dislocations, which in natural crystals are oriented in many different directions, causing an irregular distribution of microstress. There have been numerous theoretical studies of the magnetoelastic interaction between stress fields of line and planar defects and the rotated spins in a domain wall [*Stacey and Wise*, 1967; *Träuble*, 1969; *Xu and Merrill*, 1990, 1992; *Moskowitz*, 1993].

Coercivities due to wall pinning by point, line and planar defects are usually less than nucleation fields because nucleating a new domain requires a large rotation of $\mathbf{M}_s$ against anisotropy forces in some region of an existing domain. Primary nucleation usually occurs at a sharp corner where the demagnetizing field is locally enhanced [*Dunlop et al.*, 1990], either on an internal boundary, such as a void or crack [*Özdemir et al.*, 1995], or at the crystal surface [*Goodenough*, 1954; *Craik*, 1964].

The temperature dependence as well as the magnitude of coercivity is different for nucleation and various types of defect pinning. Nucleation leads to a coercivity $H_c \propto K/M_s$, where K is the predominant anisotropy constant. Wall pinning due to reduction of wall area by an amount ΔS results in $H_c \propto \Delta E_w/M_s$, where $\Delta E_w = c\Delta S(AK_1)^{1/2}$ (A is exchange constant, and c is a constant whose value depends on the type of wall: 180°, 109° or 71°). In the case of impedance of wall motion by Néel spikes, H_c is controlled by a balance between E_m and E_w. Finally, pinning due to stress fields of dislocations or planar defects gives $H_c \propto \lambda/M_s$, where λ is magnetostriction constant [*Träuble*, 1969]. *Hodych* [1982, 1990] finds the latter dependence to be dominant in many magnetite-bearing rocks, implying control of coercivity by internal stresses due to line or planar defects. In the present paper, we report new $H_c(T)$ data that refine the analysis.

In addition to making a quantitative comparison between measured H_c and values predicted by theories of wall nucleation and pinning, our purpose in the present research is to demonstrate experimentally the interaction of domain walls with various types of defects in magnetite. Although there has been much theorizing and some possibly relevant observations have been made in nickel [e.g., *Iwata and Yamamoto*, 1956], there is an almost total lack of direct observations of domain structures associated with defects in magnetite.

Experimental Methods and Sample Characterization

We observed domain structures on a 3 mm octahedral crystal of magnetite. The crystal was oriented using a laser beam and then sectioned parallel to {110} and {111} crystal planes (triangles ABC and ADE, respectively, in Figure 2). Following mechanical polishing, a final polishing using amorphous silica solution resulted in very smooth, strain-free surfaces. For details of the sample preparation, see *Özdemir et al.* [1995].

Domain walls were observed by the Bitter technique using bright-field microscopy on a Nikon-Optiphot microscope. In the Bitter method the viewing plane is decorated with colloidal ultrafine magnetite particles, which become concentrated above surface intersections of domain walls where field lines enter or leave the crystal. Walls can be identified as 71°, 109° or 180° by their angles of intersection [e.g., see *Özdemir et al.*, 1995]. Since walls bisect the angle between domain magnetizations, the directions of $\mathbf{M}_s$ vectors within domains are easily inferred. The sense of each $\mathbf{M}_s$ vector can be determined by noting which domains enlarge when a field $\mathbf{H}_0$ is applied. The "ghost" lines in Figure 1 mark positions of walls before such a field change.

Before orienting the crystal, room temperature saturation hysteresis parameters were measured with a vibrating sample magnetometer. Our crystal contains some nonmagnetic impurities, resulting in an observed $M_s = 86$ A m^2/kg, less than $M_s = 92$ A m^2/kg for pure Fe_3O_4. The saturation remanence ratio $M_{rs}/M_s = 0.003$ and the coercivity ratio $H_{cr}/H_c = 22.6$ are typical of large MD grains. High-temperature hysteresis parameters were measured on a companion crystal and will be discussed in a later section. The Curie temperature determined in this way was $T_C = 585$°C (see Figure 12), indicating pure magnetite.

A small chip of the crystal was given a saturation remanence in a field of 2.5 T at 5 K and then warmed in zero field to 300 K. The remanence decreased sharply around 122 K [see *Özdemir et al.*, 1995, Figure 4], the Verwey transition temperature. Since the Verwey transition would be broadened or suppressed by small amounts of oxidation or cation substitution [*Özdemir et al.*, 1993], the crystal is stoichiometric magnetite.

X ray diffraction using a Gandolfi camera with Cu Kα radiation and a silicon standard was carried out on another chip. The measured X ray cell edge was 8.39 ± 0.01 Å, in good agreement with the standard value of 8.396 Å for magnetite (American Society for Testing and Materials data file 19-629).

The {111} octahedral crystal surface was examined with an X ray microanalyzer using a beam current of 100 μA at 20 kV. Backscat-

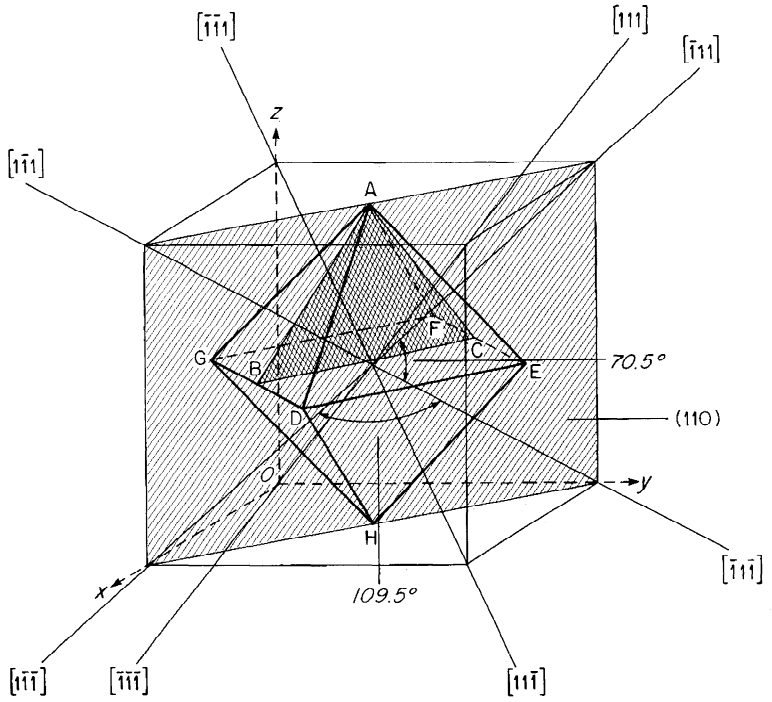

Figure 2. Sketch of a magnetite octahedron, showing the (110) plane (hatched) and eight <111> directions of easy magnetization.

tering was used to eliminate the X ray brightness of magnetite. Inclusions were easily detected in this way. The relative contents of Mg, Al, Si, and Fe determined by X ray energy dispersive analysis allowed us to identify the impurities as chlorite and biotite.

Domain Observations on a {110} Crystal Plane

In magnetite, on a strain-free {110} surface, $\mathbf{M}_s$ vectors lie along either of two sets of surface-parallel <111> easy directions, thereby minimizing both magnetostatic energy E_m and magnetocrystalline anisotropy energy E_a. As a result, 71°, 109°, and 180° walls can form with equal ease. No magnetic poles or demagnetization structures should appear on the viewing surface, and the domain patterns observed are representative of the interior domain structure.

Demagnetizing Structures Around Inclusions and Wall Pinning

Figure 3 illustrates large domains with simple shapes and straight boundaries. The 180°, 109°, and 71° walls are all clearly defined, and the $\mathbf{M}_s$ vector of each domain lies along one of the four <111> directions in the plane of view. Large spike domains at the bottom and top left are probably due to crystal defects.

A feature of interest is the pair of spike domains that form within a body domain around a 1.7 μm diameter inclusion. These spikes have the form predicted by *Néel* [1944]. Néel pointed out that magnetic poles would appear on the surface of a bare inclusion within a domain, causing a large increase in E_m. A local domain structure, as in Figure 3, would redistribute the poles over the larger surface area of the spikes. The reduction in E_m outweighs the added wall energy E_w.

Figure 4 is another example of body domains with simple geometries, typical of the crystal interior. The domains are magnetized along [$\bar{1}$11] and [1$\bar{1}$1] axes and are separated by 71°, 109°, and 180° walls. The walls are planar (i.e., straight when viewed in section) and parallel. A series of spike domains have formed on one of the 180° walls, presumably to offset local poles around crystal defects.

An interesting feature in Figure 4 is the pinning of a 71° wall to a rod-shaped inclusion through a spike domain. The 71° wall is offset to the left with respect to its extension above the middle of the photograph, its motion having been impeded by the attached truncated spike domain. In a suitably oriented applied field $\mathbf{H}_0$, the 71° wall will be driven to the right and the Néel spike will become less truncated. Eventually, the wall will escape via a Barkhausen jump to the right, leaving behind a pair of isolated Néel spikes. The rupture process, requiring a critical value of $\mathbf{H}_0$, is one source of coercivity.

Figure 5 illustrates a more complicated pinning of a 71° domain wall to an inclusion through a chain of closure domains. This inclusion, like those in Figures 3 and 4, would generate surface poles, but with a less uniform distribution because of the irregular shape of the inclusion. Thus the demagnetizing structures that appear are more complicated: a large spike domain joined to the inclusion by a small closure domain on the left, and a chain of five small and large closure domains on the right. Notice that the 71° wall makes a large bend locally to accommodate the closure domain at the end of the chain. The sizes and shapes of the supplementary domains flanking the inclusion are controlled by the balance between magnetostatic and wall energies. The spike and the chain of closure domains have grown so long that overall E_m can almost be neglected in comparison with E_w, but the 71° wall remains firmly attached.

Figure 6 gives another example of complicated arrangements of closure and spike domains formed around inclusions of irregular shape in such a way that no poles appear at the free surfaces or interfaces. The body domains in this case are magnetized along a single set of easy directions, that is, [1$\bar{1}$1], and are bounded by parallel 180° walls. The 71° and 109° walls are confined to the closure domains flanking the inclusions.

In the center of the photomicrograph, a 6 μm square inclusion

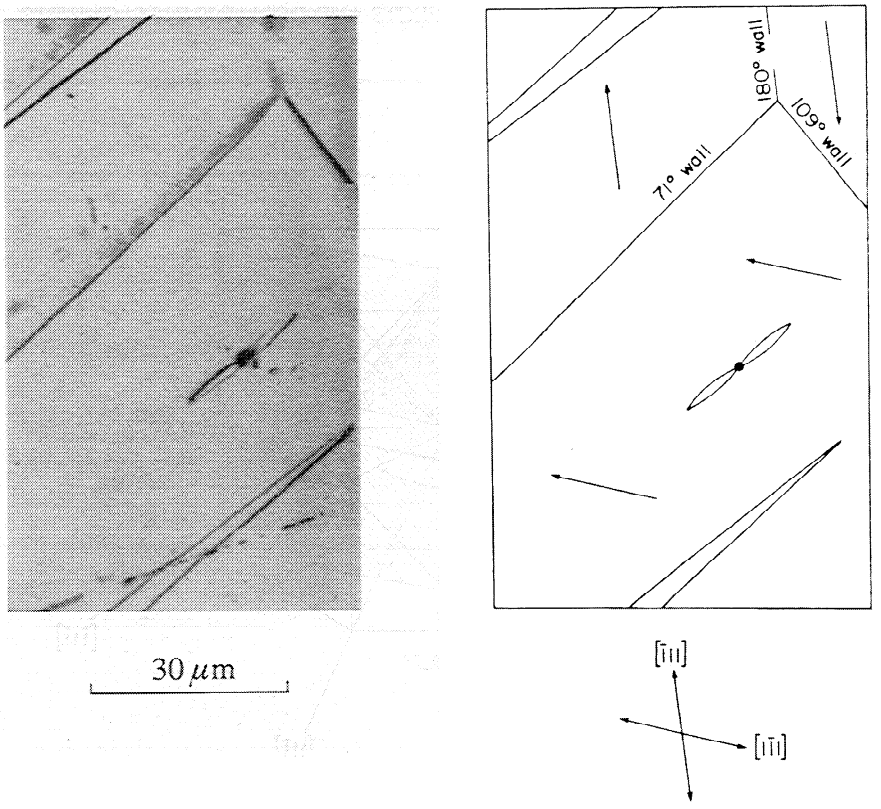

Figure 3. Domain patterns observed on a {110} surface away from the crystal edge and inferred domain magnetization directions. All $\mathbf{M}_s$ vectors are parallel to the viewing surface. Notice the domain structures around an inclusion within the body domain. A pair of spike domains around an inclusion reduces the magnetostatic energy of the system. The oblique line near the bottom of the photograph is a scratch not completely removed by polishing.

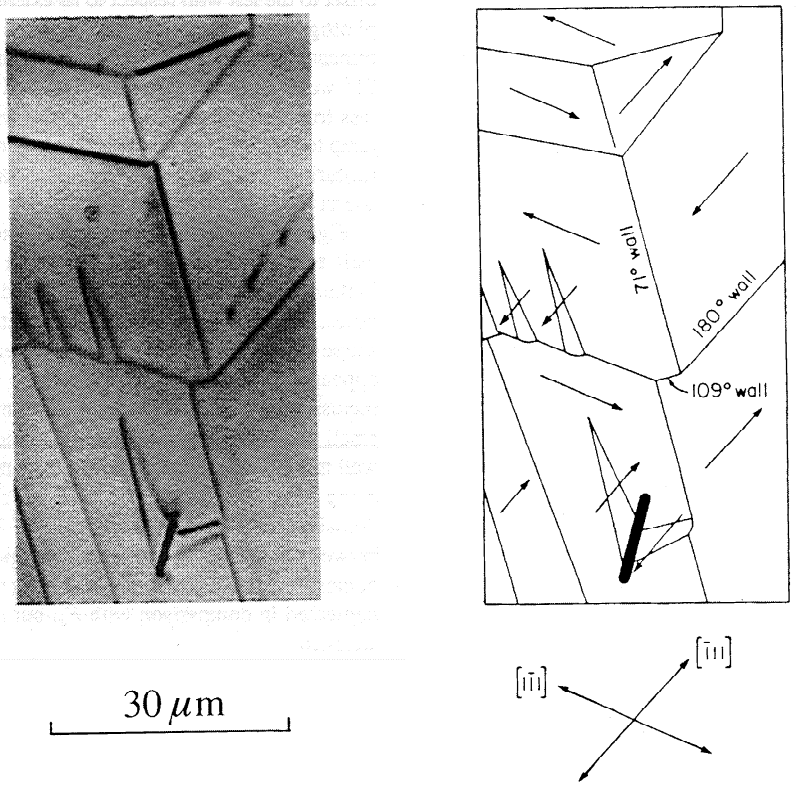

Figure 4. Domain patterns observed on a {110} surface. The body domains are magnetized along $[1\bar{1}1]$ and $[\bar{1}11]$ easy directions and are separated by 71°, 109°, and 180° walls. Notice the interaction of the 71° wall with a rod-shaped inclusion through a truncated Néel spike.

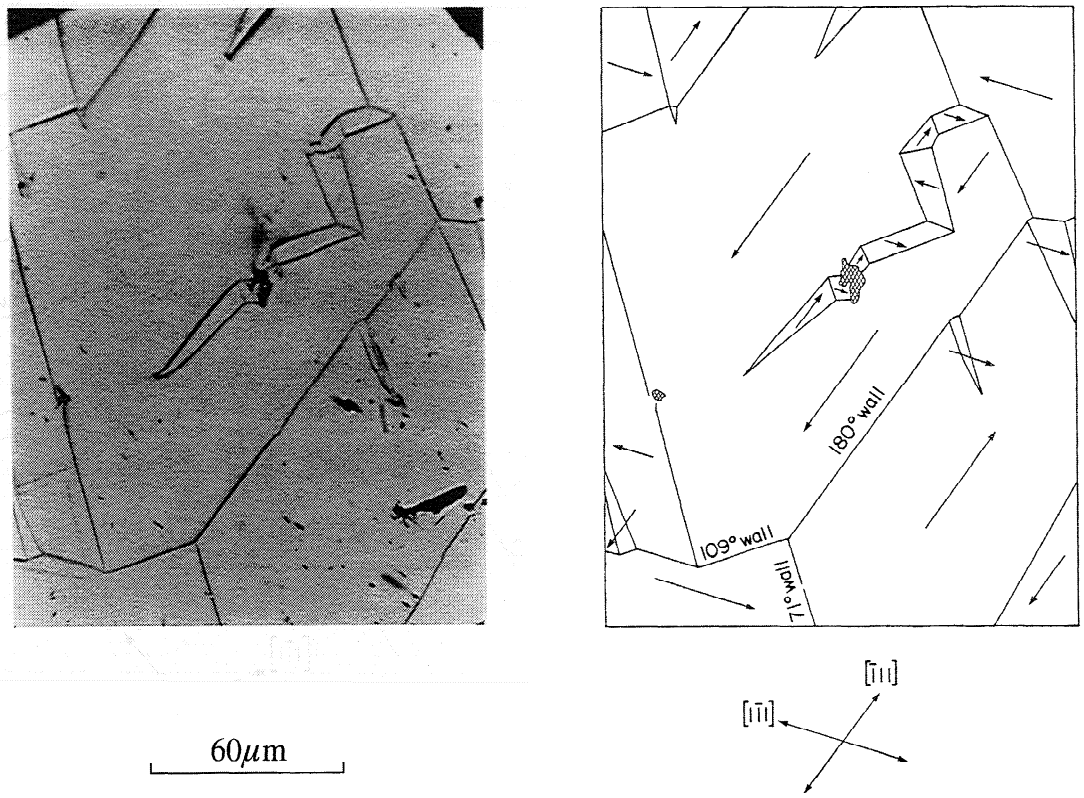

Figure 5. Pinning of a 71° domain wall to an inclusion through five closure domains ({110} viewing surface). The nonmagnetic inclusion acts as a "hole" in the uniformly magnetized domain, with the result that poles appear on the boundary of the inclusion. The magnetostatic energy would be quite large without the closure domains and the reversely magnetized spike domain anchored to the opposite side of the inclusion. The domain patterns show the process just before the connection between the closure domains and the 71° wall is broken. The retardation of the wall is the mechanism of coercivity in the crystal.

within an alteration zone is encircled by four closure domains, which complete the flux circuit between oppositely magnetized body domains and eliminate poles. At the same time, the inclusion with its ring of closure domains links together two sections of a long 180° Bloch wall. The 180° wall is very effectively pinned because any displacement on its part would disrupt the circle of closure domains and greatly increase E_m. An interesting arrangement is the attachment of the closure domain ring to the next lower 180° wall through a tubular domain. This wall too is pinned, although less effectively than its neighbor above.

Another striking observation is the pinning of the 180° Bloch wall at the lower left to an elongated defect zone through a pair of closure domains, one capped by a long reversely magnetized spike. The other end of this 180° wall terminates in a closure domain at the edge of the photograph.

Colloid Gaps: Evidence for Line Defects?

There are a series of "colloid gaps" in the Bitter images of the walls in Figure 6. These gaps are crystallographically oriented and are not due to scratches unremoved by polishing (an example of such a scratch appears in Figure 3a). The observed gaps form several straight lines, marked AB, CD, EF, cutting across the body domains and also crossing closure domains and the large demagnetizing spike. The colloid gap lines are parallel to one another and to the [$\bar{1}$11] crystallographic axis. Similar observations were reported by *Özdemir et al.* [1995].

Physically, the boundaries between different body domains and between body and closure domains cannot be discontinuous. Spins must rotate to link adjacent domains. However, if the spins locally rotate parallel to the viewing plane, rather than perpendicular to it as in a 180° Bloch wall, flux leakage from the crystal will be reduced and colloid particles will not be so strongly attracted. The likeliest explanation of the observed colloid gaps is a set of three underlying line defects such as dislocations oriented along [$\bar{1}$11] whose stress fields locally deflect spins in the walls so that they are approximately parallel to the plane of view.

Other interesting features in Figure 6 (see also Figure 1) are the kinks in the 180° domain walls (marked a, b, c) and also in the demagnetizing spike (d). The kinks probably mark the locations of Bloch lines separating segments of the wall with opposite senses of spin rotation or places where Néel caps switch direction along a wall with one sense of spin rotation [*Xu and Dunlop*, 1996]. The kinks are not obviously related to defects. However, *Moskowitz et al.* [1996] report that Bloch lines in their magnetite grains nucleate and pin at specific locations, which are different after repeated AF treatments.

Bowing of Domain Walls

Figure 7a shows body domains bounded by straight 180°, 109° and 71° walls, and subsidiary closure and spike domains along the boundary of a large chlorite inclusion about 150 μm in size, in the interior of the magnetite crystal. The $\mathbf{M}_s$ vectors of the domains, large or small, lie along either [1$\bar{1}$1] or [$\bar{1}$11] easy axes in the plane of view. Colloid gaps and kinks in walls are also visible.

A novel feature in Figure 7a is the curvature of domain walls in a small (≈15 μm) triangular magnetite grain encapsulated by the

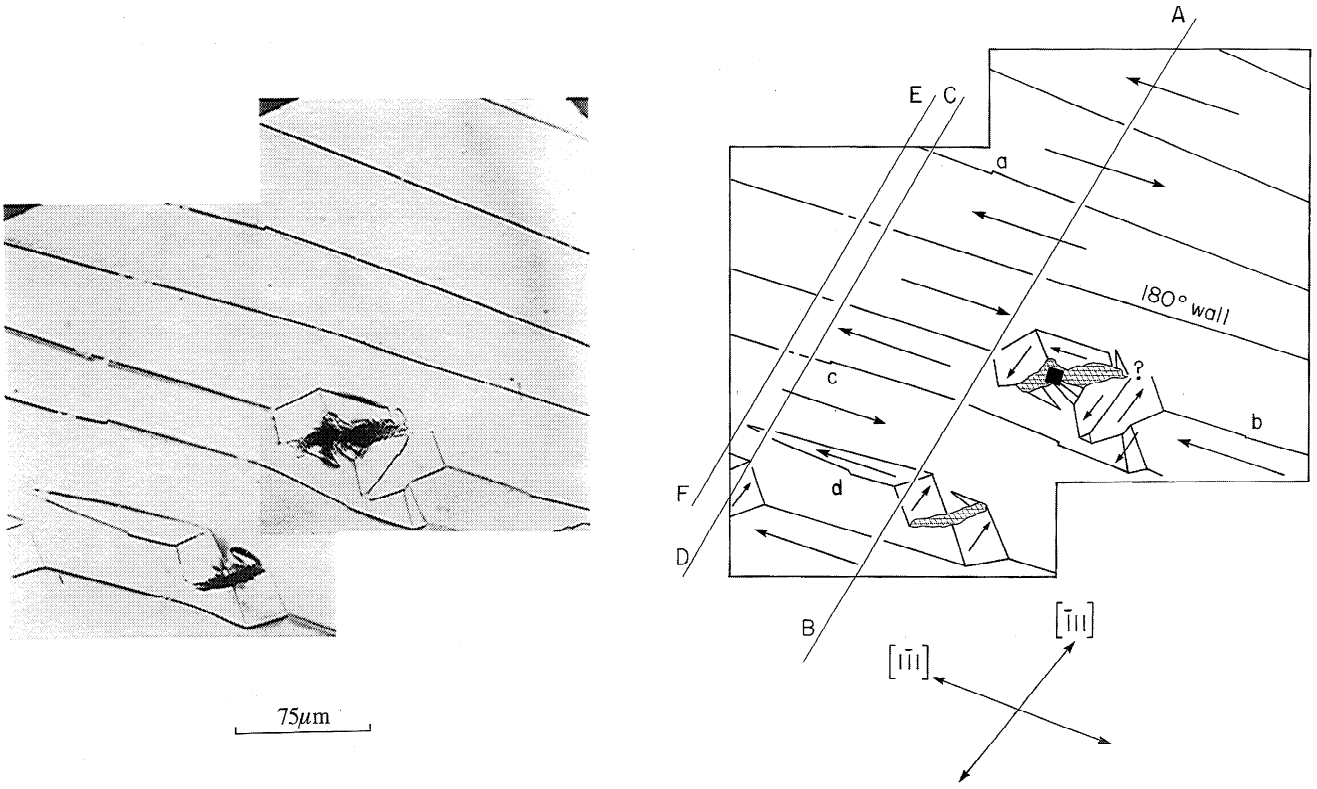

Figure 6. Effect of crystal defects on the domain structure of magnetite. Domain patterns observed on a {110} plane away from crystal boundaries show the interaction between two chemically altered regions and 180° domain walls via closure domains magnetized parallel to [1$\bar{1}$1] and [11$\bar{1}$] easy axes. There are "colloid gaps" in the walls which form several lines (marked AB, CD, and EF) cutting the 180° body domain walls and also crossing closure domains and demagnetizing spikes. The three lines are parallel to one another and to [$\bar{1}$11], suggesting crystallographically oriented line defects below the viewing surface. Notice also the kinks in 180° walls, labelled a, b, c, d.

chlorite. The grain contains four 180° domains, approximately the expected equilibrium number (see Appendix A). The walls are anchored at pinning sites on the grain boundary and have deformed by bending like an arch (Figure 7b). The magnetite grain shares one edge with an altered region in which magnetite has been oxidized and replaced by hematite. Lattice mismatch with the hematite and pressure from the surrounding chlorite produce internal stress in the magnetite grain, which in turn causes the walls to bow.

Although wall bowing caused by stress was proposed by *Kersten* [1956], it has never before been observed in magnetite, probably because quite high stress concentrations are required to offset the magnetostatic energy E_m created by poles, which appear where the $\mathbf{M}_s$ vectors intersect the curving wall. A full calculation appears in a later section.

Also of note in Figure 7a are the large reverse spike domain magnetized along [1$\bar{1}$1] (top left), bounded on its upper side by hematite and chlorite, and two spike domains along the boundary with a chemically altered region in the top right corner. In both cases, the altered region or inclusion forms a magnetic boundary on which surface poles with density $\mathbf{M}_s \cdot \hat{\mathbf{n}}$ will appear. E_m is much reduced by spreading the poles over the large surface area of the spikes.

The domain patterns in Figure 8a were observed along the edge (AB in Figure 2) where the (110) viewing plane (triangle ABC) intersects the (1$\bar{1}$1) crystal surface (triangle ADG). The closure domains are symmetric in form and bounded by pairs of ≈90° walls. One wall of each pair gathers much more colloid than the other, indicating a concentration of poles. $\mathbf{M}_s$ in the body domains is along [1$\bar{1}$1], almost at right angles to the crystal edge, while $\mathbf{M}_s$ in the closure domains is rotated away from the [1$\bar{1}\bar{1}$] easy direction so as to be more nearly parallel to the surface, thus reducing surface poles and magnetostatic energy. The magnetization directions and the origin of the uneven concentration of colloid have been discussed in detail by *Özdemir et al.* [1995].

The most striking feature of Figure 8 is the bending of the 180° wall at the left side of the micrograph. The wall is deformed into a large arc, confirming predictions [*Néel*, 1946; *Kersten*, 1956] that domain walls should be flexible rather than rigid. Notice the greater accumulation of colloid near the top of the photograph where the wall makes the largest angle with [1$\bar{1}$1], resulting in the highest pole density $\mathbf{M}_s \cdot \hat{\mathbf{n}}$.

Figures 8a and 8b also show a chain of spike and closure domains flanking a rod-shaped inclusion and interacting with the bowed wall. The wall is definitely pinned to the chain: it bends locally by a large angle where it meets the tubular domain forming the last link in the chain. In fact, this local pinning is so strong that it, rather than some distributed internal stress, is probably responsible for the bending of the wall. The inclusion, via its chain of closure domains, has effectively plucked the wall to one side like a violin string.

Discussion

Our observations show that domain structures in magnetite are very sensitive to crystal imperfections such as inclusions, grain

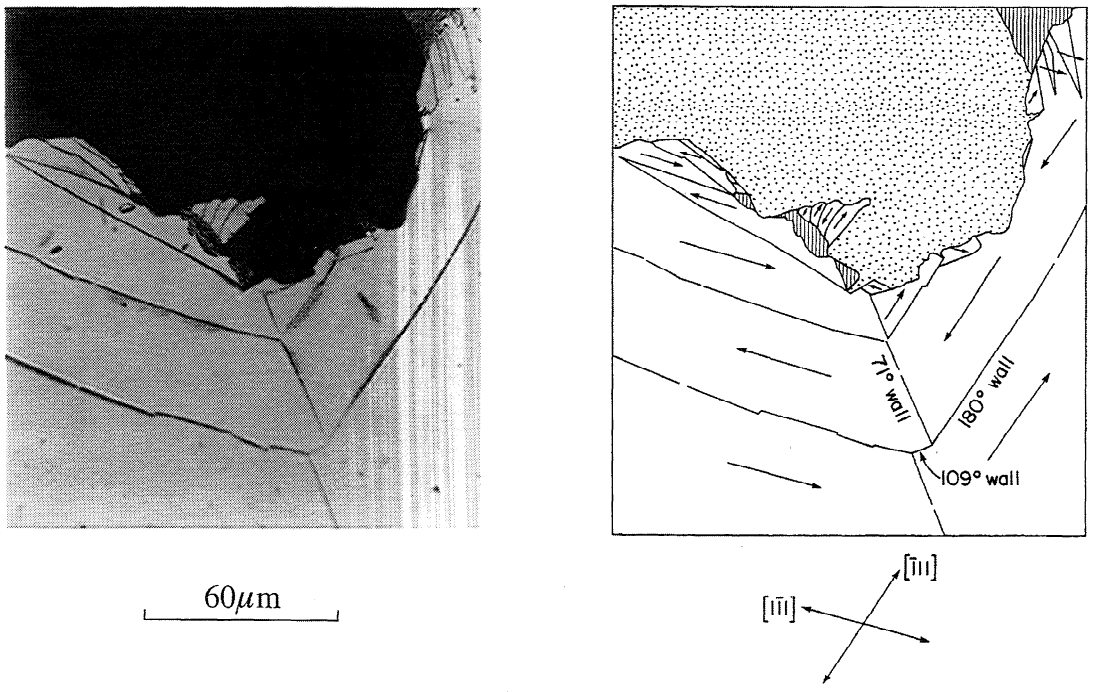

(a)

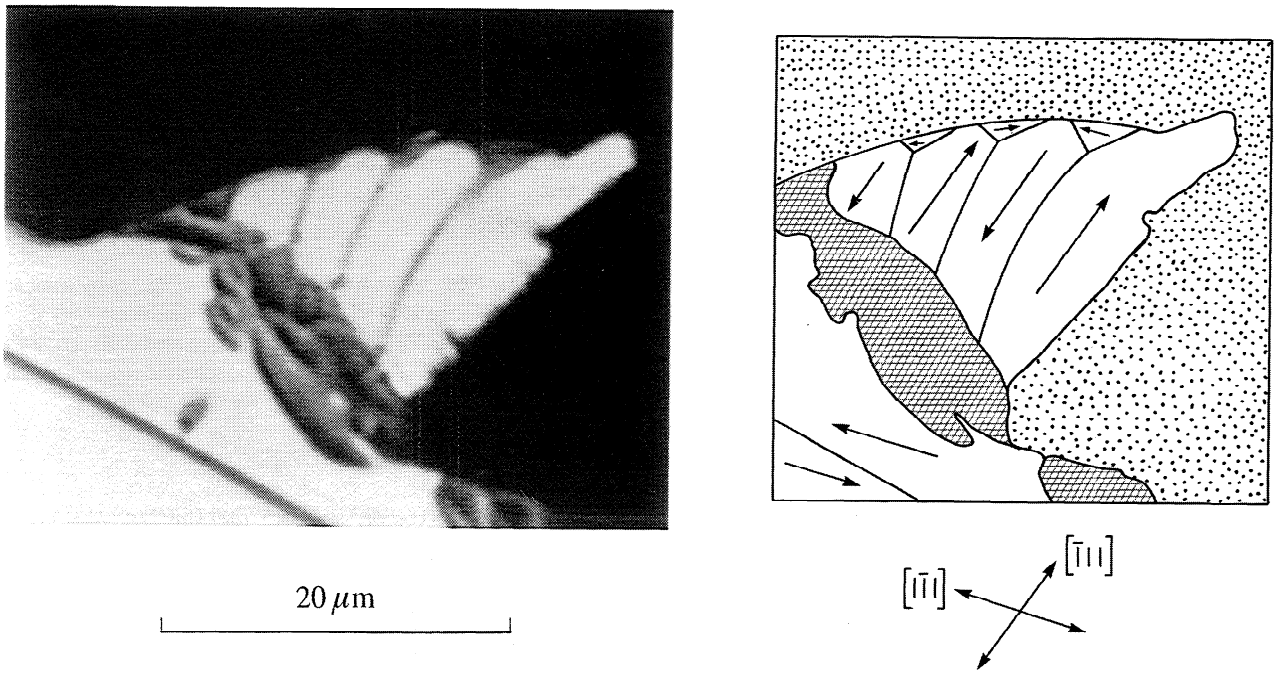

(b)

Figure 7. (a) Domain patterns around a large chlorite inclusion, viewed on a {110} surface. One large and two smaller spikes have formed with their bases on oxidized zones at the magnetite/chlorite boundary. Notice also the domain patterns on a small triangular magnetite grain encapsulated in the chlorite and bounded on its left side by hematite. (b) The magnetite grain is 15 μm in size and has four domains with magnetization along [$\bar{1}$11] and [1$\bar{1}\bar{1}$]. The 180° walls are pinned at sites on the grain boundary and have deformed by bending like an arch as a result of stress from the surrounding chlorite and hematite. The axis of each curved wall is normal to the domain magnetizations, so that positive and negative magnetic poles must appear on the bent portions of the wall, producing substantial demagnetizing energy. This observation emphasizes that domain walls in magnetite can be flexible and are not always rigid and planar as assumed in most theoretical treatments.

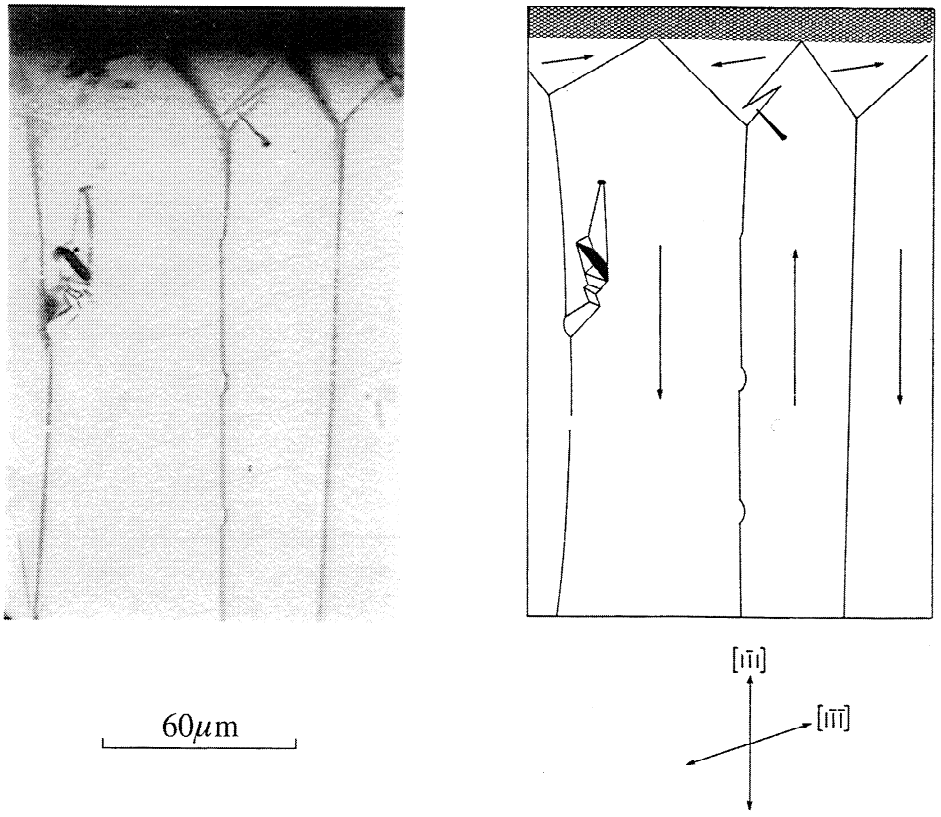

(a)

Figure 8. (a) Body and closure domains formed at the edge of the single crystal where the (110) viewing plane intersects the (1$\bar{1}$1) crystal surface. Notice the bowing of the left-hand Bloch wall as a result of its pinning to a nonmagnetic inclusion through a chain of closure domains. (b) Enlargement of the closure domain structures arising from the interaction between a 180° wall and a nonmagnetic inclusion. A large reverse spike domain on the other side of the inclusion helps minimize the magnetostatic energy.

boundaries, cracks, line defects, chemical alterations, and the internal stresses resulting from these defects. Our experimental results suggest that stray fields due to pole formation will be avoided as far as possible, on the surface as well as within the body of magnetite crystals. Spike and closure domains are the favored structures for reducing magnetostatic energy E_m. Because M_s is much larger in magnetite than in other terrestrial magnetic minerals, $E_m \propto M_s^2$ is the dominant energy in crystals of all sizes and these conclusions are likely to be quite general.

Néel Spikes

In pioneering theoretical work, before magnetic domain patterns had been observed directly, *Néel* [1944] predicted that spike domains should form at the surface of non-magnetic inclusions in order to spread magnetic poles over a large area and reduce the magnetostatic energy E_m. The reduction in energy is substantial, as we now illustrate, using the spikes (of total length 21 μm) flanking a d= 1.7 μm diameter cavity in Figure 3 as an example. The spikes are bounded by 71° walls and, by superposition, are equivalent to a region of uniform magnetization $2M_s$ sin (71°/2) parallel to the spike axis added to a uniformly magnetized body domain. We have made the assumption that poles on the cavity boundary have been eliminated by closure domains too small to resolve by the Bitter method (otherwise there would be no advantage to introducing spike domains) and that the volume of the cavity can be neglected compared to the volume of the spikes.

Following Néel, we approximate the pair of spikes by a spheroid of length kd, where k= 21/1.7 = 12.35, and diameter $(2/\pi)^{1/2}d$. The spheroid volume is $V = kd^3/3$ and its surface area is $A = (\pi^3/8)^{1/2}kd^2$. The demagnetizing factor of an elongated spheroid magnetized along its long axis is $N_{cgs} \approx (8/k^2)\{\ln[(2/\pi)^{1/2}k] - 1\}$, and so

$$E_m = \tfrac{1}{2}\mu_o VN[2M_s \sin(71°/2)]^2$$

$$E_m \approx (\mu_o/4\pi)(16d^3M_s^2 \sin^2 35.5°/3k)\{\ln[(2/\pi)^{1/2}k] - 1\}. \quad (1)$$

When we substitute values of d and k as well as M_s = 480 kA/m for magnetite, we obtain $E_m = 21.2 \times 10^{-15}$ J.

The added wall energy is approximately

$$E_w = \gamma_{71}A = \gamma_{71}(\pi^3/8)^{1/2}kd^2, \quad (2)$$

where γ_{71} is specific energy of a 71° wall. From *Lilley* [1950], $\gamma_{71} \approx 0.5(A|K_1|)^{1/2} = 0.21$ mJ/m^2, after substituting $K_1 = -13.5$ kJ/m^3 and $A = 13.3 \times 10^{-12}$ J/m [*Heider and Williams*, 1988]. From this we obtain $E_w = 14.8 \times 10^{-15}$ J. The overall energy created by adding the spike pair to a uniform body domain is $E_m + E_w = 36.0 \times 10^{-15}$ J.

If no spikes were present, poles would appear on the walls of the cavity, which by superposition is equivalent to a cube of magnetization $-M_s$ added to a uniform body domain. The demagnetizing factor N_{SD} for a uniformly magnetized cube is 1/3 (SI) or 4π/3 (cgs). Thus the energy created by adding a cavity to a uniform body domain is

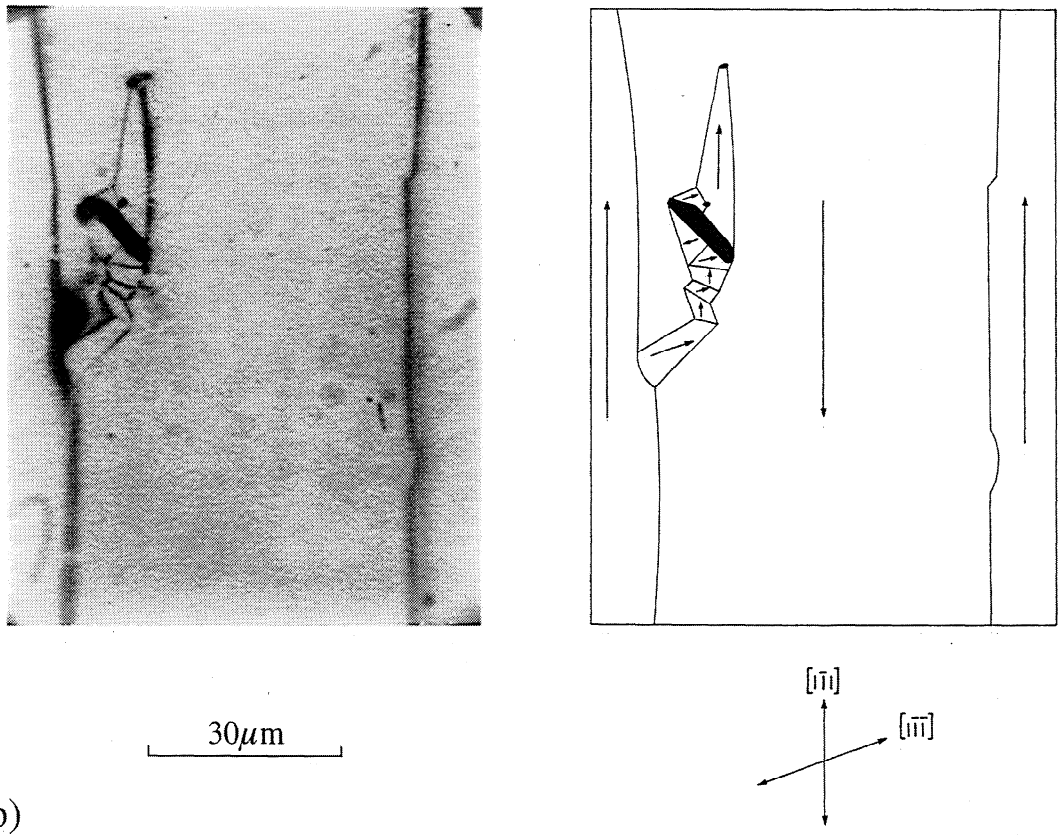

Figure 8. (continued)

$$E_m = \tfrac{1}{2}\mu_o d^3 N_{SD} M_s^2 = 237 \times 10^{-15} \text{ J}. \quad (3)$$

The energy of the bare cavity is reduced a factor ~7 by introducing the spike domains.

Bowing of 180° Bloch Walls

In order to simplify the calculation of energy barriers resulting from domain wall motion in the presence of internal stresses, early theories [*Kondorsky*, 1937; *Döring*, 1939; *Kersten*, 1943] assumed rigid walls. Changes in wall orientation, shape and thickness when the wall moved to a new position were ignored. *Néel* [1946] proposed flexible walls that would bend without becoming detached from pinning sites. *Kersten* [1956] therefore modified his previous theory by assuming that walls are pinned at sites on the grain boundary and bend within the grain in response to internal stress.

Kersten assumed that the bending axis is parallel to the domain magnetizations $\pm\mathbf{M}_s$. In this case the wall normal $\hat{\mathbf{n}}$ is everywhere perpendicular to $\mathbf{M}_s$ and the pole density $\mathbf{M}_s \cdot \hat{\mathbf{n}}$ on the wall is zero. No demagnetizing energy is created because the normal component of magnetization does not change in crossing the wall. However, experimentally we observe that the bending axis is normal to $\pm\mathbf{M}_s$ (Figures 7 and 8). Then $\hat{\mathbf{n}}$ is perpendicular to $\pm\mathbf{M}_s$ at the midpoint of the wall but not elsewhere. Positive (or north) poles will form on the lower half of the wall and negative poles on the upper half (Figure 9). If the wall were to remain straight to avoid the magnetostatic energy due to pole formation, parts of it located in regions of high microstress would have high magnetoelastic energy E_s. The wall therefore assumes a shape that minimizes the sum $E_m + E_s$. We will follow *Xu and Merrill*'s [1992] theoretical treatment of one-dimensional flexure of a wall in order to estimate the internal stress responsible for our observed domain wall bowing.

Figure 9 shows a 180° Bloch wall which has bowed under internal stress σ into a circular arc of radius R. The undeformed length of the wall between its pins at either end is a and the transverse displacement of the midpoint of the wall is h. The reduction in the magnetoelastic energy when wall bows is

$$E_s = \lambda_s w a^2 \langle\sigma\rangle, \quad (4)$$

where $\langle\sigma\rangle$ is the average internal stress, $\lambda_s = 35.8 \times 10^{-6}$ is the saturation magnetostriction constant for magnetite, and w is the wall thickness ($w << a$). The reduction in E_s is offset by increases in E_m and E_w. *Xu and Merrill* [1992] estimated E_m by approximating the wall by a two-domain thin plate (demagnetizing factor N= 1 in SI or 4π in cgs). The "domains" are the upper (negative) and lower (positive) pole sheets, each with average pole density $aM_s/4R$. Thus

$$E_m = \tfrac{1}{2}\mu_o N w a^2 (aM_s/4R)^2 = \mu_o w a^4 M_s^2/(32R^2). \quad (5)$$

Xu and Merrill show that the increase in E_w can be ignored compared to E_m for magnetite. Thus the magnetoelastic energy can be balanced against magnetostatic energy, giving

$$(h/a)^2 \approx (a/8R)^2 = \lambda_s \langle\sigma\rangle / 2\mu_o M_s^2. \quad (6)$$

Using (6) with values of M_s and λ_s for magnetite, we determined levels of internal stress $\langle\sigma\rangle$ from observed values of h/a for various bowed 180° walls (Figures 6, 7, and 8). The internal stresses in most cases are in the range 7-34 MPa (Figure 10). These values are

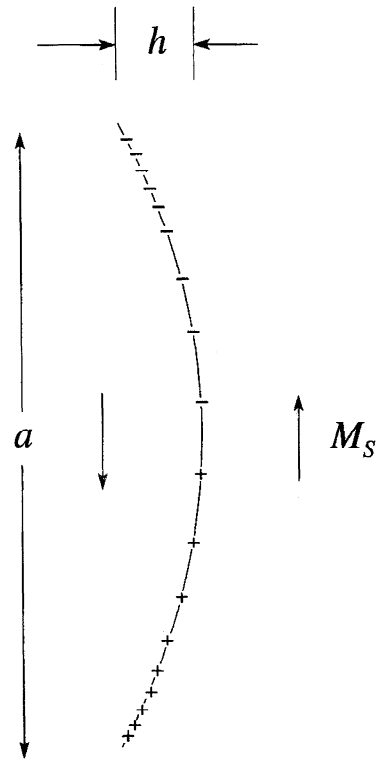

Figure 9. Bowing of a 180° domain wall in a {110} viewing plane, where h is the bulging and a is the length of the wall (redrawn after *Xu and Merrill* [1992]). The direction of magnetization in each domain is in the plane of view and normal to the wall bending axis. Thus the normal component of $\mathbf{M}_s$ is not continuous across the wall, and magnetic poles appear, as indicated by the plus and minus signs.

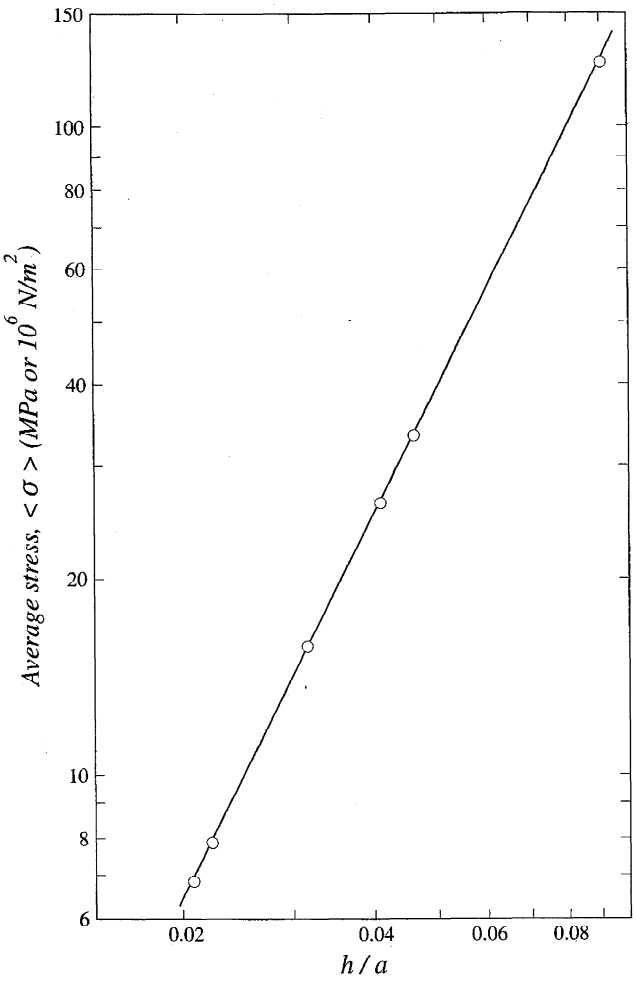

Figure 10. Variation of average internal stress <σ> as a function of h/a for various curved walls observed on a {110} plane of our magnetite crystal (h and a are defined in Figure 9). Circles are measurements of h/a from Figures 6, 7b, and 8a. The highest value of h/a and <σ> is for the strongly bowed wall in the 15 μm magnetite grain encapsulated in chlorite (Figure 7b).

probably upper bounds because we cannot view the third dimension and the wall area in (4)-(6) should probably be less than a^2. There is one very high value, approaching 150 MPa, for a strongly curved wall in the triangular magnetite grain in Figure 7b. As mentioned earlier, this grain is under considerable stress because of lattice mismatch with hematite along its lower boundary and matrix pressure from the surrounding chlorite elsewhere.

Microcoercivity Resulting From Wall-Defect Interaction

The pinning of a 71° wall by an inclusion and its associated spikes (Figure 4) permits us to make an estimate of microcoercivity resulting from wall-defect interaction. Figure 11 sketches the wall and spike configurations initially and just after the wall has snapped loose from the spike as a result of increasing the field $\mathbf{H}_0$ in the direction of $\mathbf{M}_s$ in the right-hand domain. The critical field required to free the wall from the inclusion is the microcoercive force h_c. According to *Döring* [1938] and *Néel* [1944], h_c is given by

$$h_c \approx 5/4\ (\pi^3/8)^{1/4}\ (\gamma_w/M_s r), \tag{7}$$

where r is the radius of inclusion. The inclusion in this case is rod shaped. We take r= 2 μm to be its equivalent radius. Substituting $\gamma_w = \gamma_{71}$ = 0.21 mJ/m^2, we find h_c= 0.54 mT.

In the next section we present evidence that the main source of coercivity in our crystal is magnetoelastic interaction between walls and the stress fields of line or planar defects, rather than the basically magnetostatic pinning of walls to volume defects like inclusions. Nevertheless, it is interesting that the bulk coercive force H_c, an average value of h_c for the crystal, was measured to be about 0.5 mT.

Temperature Dependence of Coercive Force

We also measured H_c and M_s as a function of temperature T in order to understand the origin of coercivity in our magnetite crystal. The measurements were made with a Princeton Measurements Corporation Micro VSM at the Institute for Rock Magnetism, University of Minnesota, on a 4 mm companion crystal. Hysteresis was measured at 20°C intervals from room temperature to 600°C. A continuous jet of helium passing through the furnace prevented chemical alteration.

The temperature variations of H_c and M_s are shown in Figure 12. M_s varies as $(T_c - T)^{0.4}$, as found by *Pauthenet* [1952], and disappears at the Curie point T_C = 585°C. As discussed in the Introduction, many different temperature variations of H_c are possible, depending on the mechanism of microcoercivity [see *Moskowitz,* 1993, Table 2]. The most rapid variation is

$$H_c(T) \propto K_1(T)/M_s(T) \tag{8}$$

due to domain nucleation or magnetocrystalline anisotropy pinning

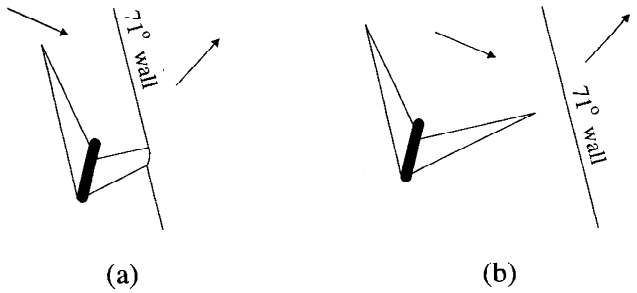

Figure 11. (a) Pinning of a 71° wall to an inclusion and its associated Néel spikes. The observed domain structure is given in Figure 4. (b) In an applied field, the wall snaps loose from its pinning site and jumps to the right.

by a planar defect, and the slowest variation is

$$H_c(T) \propto \lambda_s(T)/M_s(T) \tag{9}$$

due to pinning of walls by the stress fields of dislocations or stacking faults.

The temperature variations represented by (8) and (9) are plotted as curves 1 and 2, respectively, in Figure 12. The data of *Fletcher and O'Reilly* [1975] were used for $K_1(T)$ and the $\lambda_{111}(T)$ data of *Klapel and Shive* [1974] were used to approximate $\lambda_s(T)$. Our experimental $H_c(T)$ data vary approximately as $\lambda_{111}(T)/M_s(T)$, indicating that the coercivity in our MD crystal is mainly magnetoelastic, that is, due to pinning of magnetization by internal stress.

However, there is a small difference between the experimental data and curve 2, which probably arises in the following way. The theory leading to the $\lambda_s(T)/M_s(T)$ dependence of H_c is for a single dislocation and a constant wall width w. If w varies with T, different numbers of defects interact with the wall at different temperatures. Most theories of defect controlled microcoercivity predict that $h_c(T)$ depends on $w^m(T)$, where m depends on the number and arrangement of defects [*Träuble*, 1969; *Xu and Merrill*, 1989; *Moskowitz*, 1993]. For example, *Xu and Merrill* [1989, 1990, 1992] have shown that

$$h_c(T) \propto \lambda_{111}(T)w^{0.5}(T)/M_s(T) \tag{10}$$

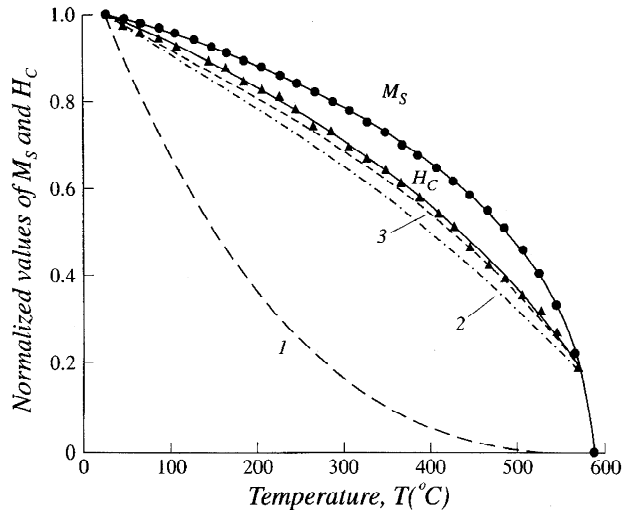

Figure 12. Measured temperature variation of normalized saturation magnetization M_s and coercive force H_c for a companion magnetite crystal (from the same locality as the one on which domain patterns were observed). Curves 1, 2, and 3 represent calculated $H_c(T)$ variations $\propto K_1/M_s$, λ_{111}/M_s and $\lambda_{111}w^{0.5}/M_s$, respectively.

and that H_c is proportional to mean microcoercivity $\langle h_c \rangle$ for high defect densities, giving

$$H_c(T) = C\,\lambda_{111}(T)w^{0.5}(T)/M_s(T), \tag{11}$$

where C is a constant independent of temperature.

The $H_c(T)$ variation of (11) is shown as curve 3 in Figure 12. The temperature dependence $w(T)$ was taken from *Xu and Merrill* [1992], who assumed that the variation of wall width with temperature in magnetite is mainly determined by stress and magnetostatic energy, rather than magnetocrystalline anisotropy which would allow a rapid and almost unlimited expansion of walls upon heating. However, instead of the room temperature wall width of 110 nm used by *Xu and Merrill* [1992, Figure 5], we adopted the experimental value of 210 nm observed by *Proksch et al.* [1994] using magnetic force microscopy on an oriented magnetite crystal. The calculated $H_c(T)$ values agree very well with our experimental results, indicating that wall pinning by crystal defects in natural magnetite controls coercivity and magnetic stability, at least in our crystal. The data of *Hodych* [1982, 1990] suggest that this conclusion is general.

Chemically Altered Regions

Regions in which magnetite has been oxidized to hematite act as magnetic boundaries because hematite is only weakly ferromagnetic. A case in point is the formation of closure domains at the boundaries of oxidized zones in Figures 5 and 6, whose purpose is to redistribute poles that would otherwise appear with high density on the boundary. Similarly, the sets of spikes attached to the altered zones in Figure 7a (top right) offset poles on these boundaries. As oxidation spreads through the crystal, closure and spike domains will form intricate networks, like those observed by *Özdemir et al.* [1995, Figure 6], changing both the body domain structure and the remanence of the crystal. These experimental observations provide a direct link between chemical alteration and domain structures that could result in remagnetization.

Colloid Gaps and Kinks

"Colloid gaps" are common features of 180° and other walls in magnetite. We propose that the magnetization in these colloid-free zones is parallel to the plane of view, thus eliminating surface poles and reducing stray fields which attract colloid. The colloid gaps are generally parallel to one another and to a <111> crystallographic axis (Figure 5; see also *Özdemir et al.* [1995, Figure 9]). Our interpretation is that line defects underlying the viewing plane locally deflect the spins in the walls they cross, reducing the leakage field above the wall.

Even more frequent are kinks in 180° walls, probably marking the locations of Néel cap switching or of Bloch lines, at which the direction of interior rotation of spins in the wall reverses. Similar observations were first made by *DeBlois and Graham* [1958] and interpreted by *Shtrikman and Treves* [1960], who postulated that the sign of poles on the edge of the wall, where it intersects the viewing plane, switches along the length of the wall.

Conclusions

1. Domain structures in magnetite are strongly influenced by crystal imperfections, such as inclusions and voids, grain boundaries (including cracks, sharp bends and corners), line defects (dislocations) and chemically altered regions, and by the internal stresses resulting from these defects. Our observations imply that stray fields due to pole formation at defect boundaries will be avoided as far as

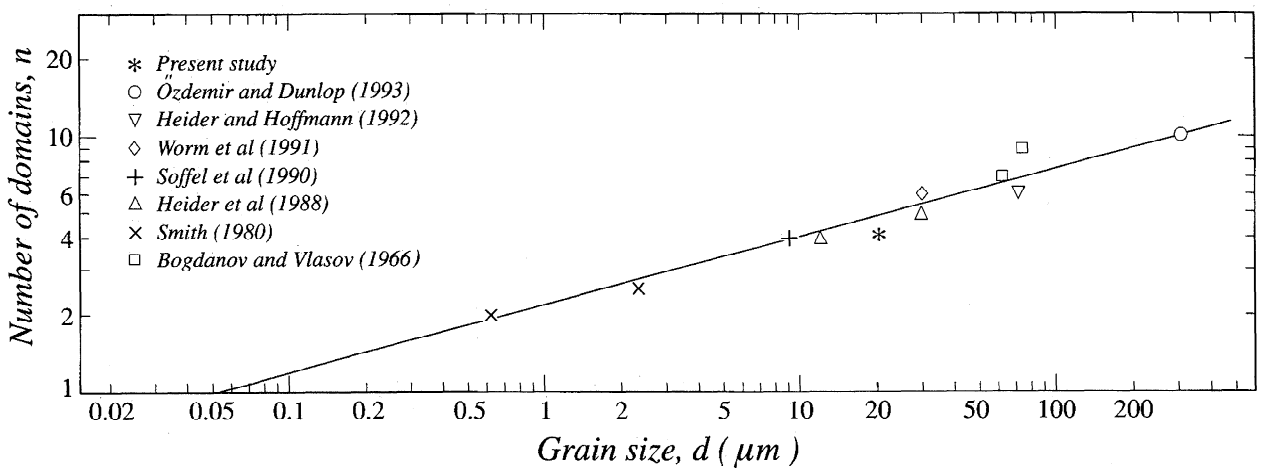

Figure A1. The number of domains observed in polished magnetite grains by different techniques: Bitter colloid (circle, squares, and asterisk), magneto-optical Kerr effect (inverted triangle, diamond), Lorentz TEM (crosses), dried colloid SEM (plus). Our observation of four domains in the 15 μm grain of Figure 7b agrees with previous data. The number of domains decreases with decreasing grain size and by extrapolation predicts a value of 0.05 μm for the critical single-domain size in magnetite.

possible, usually by the formation of closure domains and reverse spikes, which in turn can serve as domain nucleating sites.

2. Inclusions are the commonest defect in natural magnetite crystals. Isolated inclusions within body domains generally have attached Néel spikes or chains of closure domains which serve to dilute the free poles associated with the inclusion and thereby reduce magnetostatic demagnetizing energy. For example, a simple calculation shows that a pair of Néel spikes 21 μm in length flanking a 1.7 μm inclusion have an energy about 6 times less than the bare inclusion and its associated poles.

3. The 71°, 109°, and 180° domain walls are sometimes pinned to defects indirectly via spikes or subsidiary closure domain structures. In some cases (Figures 4 and 8) the pinning is so strong that the wall deforms by segmentation or by curving like a plucked string.

4. We observe bowing of 180° domain walls (e.g., Figure 7b),

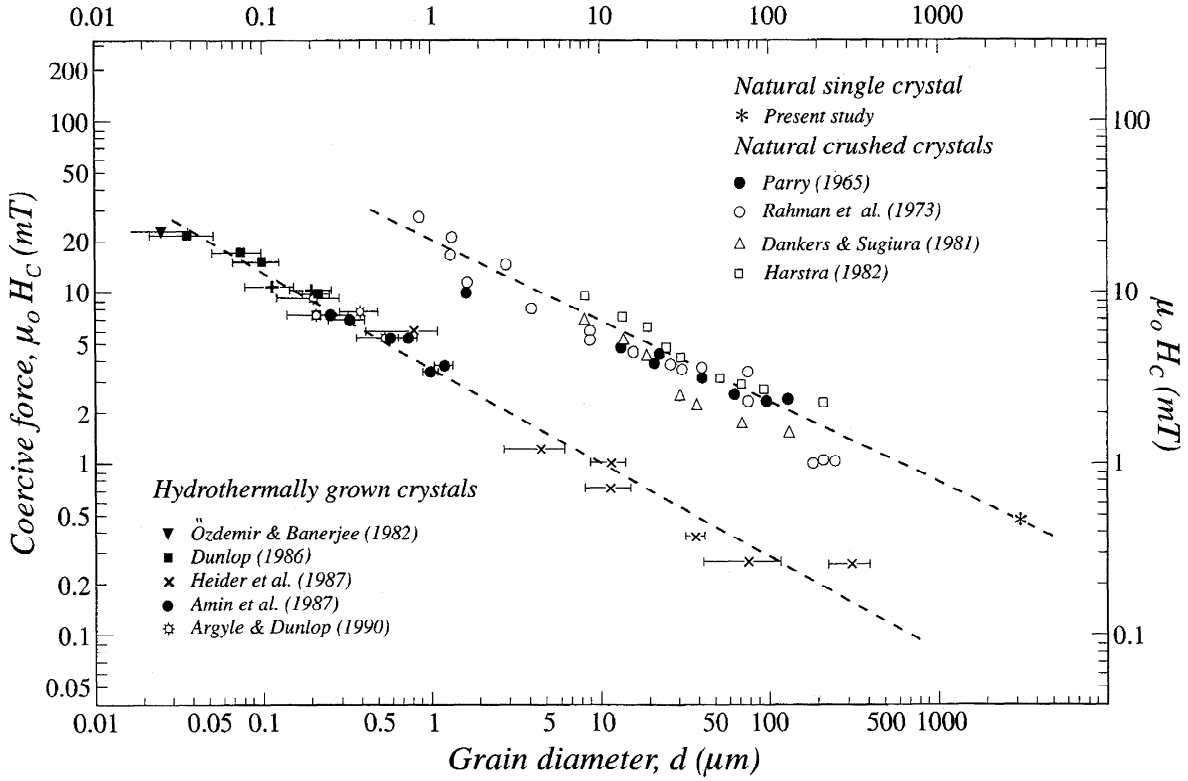

Figure B1. Experimental coercive force of our natural magnetite crystal compared with H_c data for hydrothermally grown (low stress) synthetic crystals and crushed (high stress) natural magnetites. Our crystal belongs with the high stress group.

indicating that walls can be flexible and are not always rigid as assumed in most theoretical studies. Wall bowing is also tangible evidence of the effect of internal stresses on the domain structure of magnetite. The internal stresses calculated from our observed values of the length and transverse displacement of bowed walls are in the range 7-34 MPa.

5. Wall pinning by a Néel spike flanking a rod-shaped inclusion gives a calculated value of micrococrcivity h_c= 0.54 mT. Although this value agrees well with the measured coercive force H_c= 0.5 mT of the whole crystal, it is calculated for one individual defect only and does not prove that magnetostatic pinning of walls by volume defects is the main source of bulk coercivity.

6. H_c in a companion magnetite crystal varies with temperature as $\lambda_{111}\, w^{0.5}/M_s$, as predicted theoretically for domain wall pinning by dislocations in a material with high defect density. This result indicates that coercivity in multidomain magnetite is controlled mainly by crystal defects.

Appendix A: Equilibrium Number of Domains

Özdemir et al. [1995, equation (3)] give an expression for the equilibrium width L_{eq} of 180° domains. We obtain the equilibrium number n_{eq} of domains by dividing the grain diameter d by L_{eq}:

$$n_{eq} = (9\lambda^2_{111} c_{44} d/4\gamma_w)^{1/2}, \qquad \text{(A1)}$$

where for magnetite, λ_{111}= 72.6 × 10^{-6}, the elastic constant c_{44}= 9.55 × 10^{10} N/m^2, and γ_w= γ_{180}= $2(A/K_1)^{1/2}$ = 0.85 mJ/m^3 [*Lilley*, 1950]. For the d≈ 15 μm magnetite grain enclosed by chlorite (Figure 7b), (A1) predicts n_{eq} = 4.5. The number of domains observed is 4.

The number of domains for this small magnetite grain is consistent with observations by many different techniques on magnetites from 0.6 μm to 300 μm in size (Figure A1). The log n versus log d line has a slope somewhat less than the ½ expected from (A1), but the line extrapolates to a reasonable value for the critical single-domain (n= 1) size: d_o≈ 0.05 μm.

Appendix B: Coercive Force and Defect Density

Figure B1 illustrates the variation of bulk coercive force H_c with grain size d in magnetite. The H_c value of our crystal falls on the extrapolated trend of values for crushed natural crystals and not on the trend for low-stress hydrothermally grown crystals. Our natural crystal has a higher defect density than synthesized crystals, and these defects are the source of coercivity, both because they pin walls and because they create regions of internal stress, causing wall bowing.

Acknowledgments. We thank Karl Fabian, Ron Merrill, Michel Prévot and an anonymous referee for useful comments. Malcolm Back and Bob Ramik donated the single crystals of magnetite. High-temperature hysteresis and low-temperature remanence measurements were made at the Institute for Rock Magnetism (IRM) at the University of Minnesota, which is operated with support from the Keck Foundation and the National Science Foundation. We are grateful to Subir Banerjee, Bruce Moskowitz, Jim Marvin, and Mike Jackson for welcoming us as Visiting Fellows at the IRM and for their help with the instruments and experiments. This research has been supported by the Natural Sciences and Engineering Research Council of Canada through research grant A7709 to D.J.D.

References

Amin, N., S. Arajs, and E. Matijevic, Magnetic properties of uniform spherical magnetic particles prepared from ferrous hydroxide gels, *Phys. Status Solidi A*, *101*, 233-238, 1987.

Argyle, K. S., and D. J. Dunlop, Low-temperature and high-temperature hysteresis of small multidomain magnetites (215-540 nm), *J. Geophys. Res.*, *95*, 7069-7083, 1990.

Banfield, J. F., P. J. Wasilewski, and D. R. Veblen, TEM study of relationships between the microstructures and magnetic properties of strongly magnetized magnetite and maghemite, *Am. Mineral.*, *79*, 654-667, 1994.

Bogdanov, A. A., and A. Y. Vlasov, The domain structure of magnetite particles, *Izv. Acad. Sci. USSR, Phys. Solid Earth*, Engl. Transl., no. 1, 28-32, 1966.

Craik, D. J., The magnetic properties of grain boundaries, in *International Conference on Magnetism Proceedings*, pp. 693-696, Univ. of Nottingham Press, Nottingham, England, 1964.

Dankers, P., and N. Sugiura, The effects of annealing and concentration on the hysteresis properties of magnetite around the PSD-MD transition, *Earth Planet. Sci. Lett.*, *56*, 422-428, 1981.

DeBlois, R. W., and C. D. Graham Jr., Domain observations on iron whiskers, *J. Appl. Phys.*, *29*, 931-939, 1958.

Dijkstra, L. J., and C. Wert, Effect of inclusions on the coercive force of iron, *Phys. Rev.*, *79*, 979-985, 1950.

Döring; W., Über das Anwachsen der Ummagnetizierungskeime bei grossen Barkhausen-Sprungen, *Z. Phys.*, *108*, 137-152, 1938.

Döring, W., Reversible processes in magnetic materials with small inner strains, *Z. Phys.*, *114*, 579-601, 1939.

Dunlop, D. J., Hysteresis properties of magnetite and their dependence on particle size: A test of pseudo-single-domain remanence models, *J. Geophys. Res.*, *91*, 9569-9584, 1986.

Dunlop, D. J., R. J. Enkin, and E. Tjan, Internal field mapping in single-domain and multidomain grains, *J. Geophys. Res.*, *95*, 4561-4577, 1990.

Fabian, K., A. Kirchner, W. Williams, F. Heider, A. Hubert, and T. Leibl, Three dimensional micromagnetic calculations for magnetite using FFT, *Geophys. J. Int.*, *124*, 89-104, 1996.

Fletcher, E. J., and W. O'Reilly, Contribution of Fe^{2+} ions to the magnetocrystalline anisotropy constant K_1 of $Fe_{3-x}Ti_xO_4$ (0<x<0.1), *J. Phys. C Solid State Phys.*, *7*, 171-178, 1975.

Geiß, C. E., F. Heider, and H. C. Soffel, Magnetic domain observations on magnetite and titanomaghemite grains (0.5-10 μm), *Geophys. J. Int.*, *124*, 75-88, 1996.

Goodenough, J. B., A theory of domain creation and coercive force in polycrystalline ferromagnetics, *Phys. Rev.*, *95*, 917-932, 1954.

Harstra, R. L., Grain-size dependence of initial susceptibility and saturation magnetization-related parameters of four natural magnetites in the PSD-MD range, *Geophys. J. R. Astron. Soc.*, *71*, 477-495, 1982.

Heider, F., and V. Hoffmann, Magneto-optical Kerr effect on magnetite crystals with externally applied magnetic fields, *Earth Planet. Sci. Lett.*, *108*, 131-138, 1992.

Heider, F., and W. Williams, Note on temperature dependence of exchange constant in magnetite, *Geophys. Res. Lett.*, *15*, 184-187, 1988.

Heider, F., D. J. Dunlop, and N. Sugiura, Magnetic properties of hydrothermally recrystallized magnetite crystals, *Science*, *236*, 1287-1290, 1987.

Heider, F., S. L. Halgedahl, and D. J. Dunlop, Temperature dependence of magnetic domains in magnetite crystals, *Geophys. Res. Lett.*, *15*, 499-502, 1988.

Hodych, J. P., Magnetostrictive control of coercive force in multidomain magnetite, *Nature*, *298*, 542-544, 1982.

Hodych, J. P., Magnetic hysteresis as a function of low temperature in rocks: Evidence for internal stress control of remanence in multi-domain and pseudo-single-domain magnetite, *Phys. Earth Planet. Inter.*, *64*, 21-36, 1990.

Iwata, T., and M. Yamamoto, Ferromagnetic domain patterns on nickel crystals, II. Domain patterns on general surfaces of unmagnetized crystals, *Sci. Rep. Res. Inst. Iron Steel Other Metals Tohoku Univ., A8*, 293-312, 1956.

Jakubovics, J. P., A. J. Lapwoth, and T. W. Jolly, Electron microscope studies of ferromagnetic ordered structures, *J. Appl. Phys.*, *49*, 2002-2006, 1978.

Kersten, M., *Grundlagen einer Theorie der ferromagnetischen Hysterese und der Koerzitivkraft*, 88 pp., S. Hirzel, Leipzig, 1943.

Kersten, M., Die Wölbung der Blochwand als Elementarvorgang reversibler Magnetisierungsänderungen (Anfangspermeabilität und ΔE-Effekt), *Z. Phys.*, *7*, 313-322, 1956.

Klapel, J. D., and P. N. Shive, High-temperature magnetostriction of magnetite, *J. Geophys. Res.*, *79*, 2629-2633, 1974.

Kondorsky, E., On the nature of the coercive force and irreversible changes in magnetization, *Phys. Z. Sowjetunion*, *11*, 597-620, 1937.

Lilley, B. A., Energies and widths of domain boundaries in ferromagnetics, *Philos. Mag.*, *41*, 792-813, 1950.

Moskowitz, B. M., Micromagnetic study of the influence of crystal defects on coercivity in magnetite, *J. Geophys. Res.*, *98*, 18,011-18,026, 1993.

Moskowitz, B. M., T. G. Pokhil, and S. K. Banerjee, Magnetic force microscopy (MFM) of pseudo-single-domain magnetite (abstract), *Eos Trans. AGU*, *77* (22), West. Pac. Geophys. Meet. Suppl., W22, 1996.

Néel, L., Effect des cavités et des inclusions sur le champ coercitif, *Cah. Phys.*, *25*, 21-44, 1944.

Néel, L., Bases d'une nouvelle théorie générale du champ coercitif, *Ann. Univ. Grenoble*, *22*, 299-343, 1946.

Newell, A. J., D. J. Dunlop, and W. Williams, A two-dimensional micromagnetic model of magnetizations and fields in magnetite, *J. Geophys. Res.*, *98*, 9533-9549, 1993.

Özdemir, Ö., and S. K. Banerjee, A preliminary magnetic study of soil samples from west-central Minnesota, *Earth Planet. Sci. Lett.*, *59*, 393-403, 1982.

Özdemir, Ö., and D. J. Dunlop, Magnetic domain structures on a natural single crystal of magnetite, *Geophys. Res. Lett.*, *20*, 1835-1838, 1993.

Özdemir, Ö., D. J. Dunlop, and B. M. Moskowitz, The effect of oxidation on the Verwey transition in magnetite, *Geophys. Res. Lett.*, *20*, 1671-1674, 1993.

Özdemir, Ö., S. Xu, and D. J. Dunlop, Closure domains in magnetite, *J. Geophys. Res.*, *100*, 2193-2209, 1995.

Parry, L. G., Magnetic properties of dispersed magnetite powders, *Philos. Mag.*, *11*, 303-312, 1965.

Pauthenet, R., Aimantation spontanée des ferrites, *Ann. Phys.*, *7*, 710-747, 1952.

Pokhil, T. G., and B. M. Moskowitz, Magnetic force microscope study of domain wall structures in magnetite, *J. Appl. Phys.*, *79*, 6064-6066, 1996.

Proksch, R. B., S. Foss, and E. D. Dahlberg, High resolution magnetic force microscopy of domain wall fine structures, *IEEE Trans. Magn.*, *MAG-30*, 4467-4472, 1994.

Rahman, A. A., A. D. Duncan, and L. G. Parry, Magnetization of multi-domain magnetite particles, *Riv. Ital. Geofis.*, *22*, 259-266, 1973.

Shtrikman, S., and D. Treves, Internal structure of Bloch walls, *J. Appl. Phys.*, *31*, 147S-148S, 1960.

Smith, P. P. K., The application of Lorentz electron microscopy to the study of rock magnetism, *Inst. Phys. Conf. Ser.*, *52*, pp. 125-128, Inst. Phys., Bristol, England, 1980.

Soffel, H. C., C. Aumüller, V. Hoffmann, and E. Appel, Three-dimensional domain observations of magnetite and titanomagnetites using the dried colloid SEM method, *Phys. Earth Planet. Inter.*, *65*, 43-53, 1990.

Stacey, F. D., and K. N. Wise, Crystal dislocations and coercivity in fine grained magnetite, *Aust. J. Phys.*, *20*, 507-513, 1967.

Träuble, H., The influence of crystal defects on magnetization processes in ferromagnetic single crystals, in *Magnetism and Metallurgy*, pp. 621-687, edited by A. E. Berkowitz and E. Kneller, Academic, San Diego, Calif., 1969.

Williams, W., and D. J. Dunlop, Some effects of grain shape and varying external magnetic field on the magnetic structure of small grains of magnetite, *Phys. Earth Planet. Inter.*, *65*, 1-14, 1990.

Williams, W., V. Hoffmann, F. Heider, T. Göddenhenreich, and C. Heiden, Magnetic force microscopy imaging of domain walls in magnetite, *Geophys. J. Int.*, *111*, 417-423, 1992.

Worm, H-U., P. J. Ryan, and S. K. Banerjee, Domain size, closure domains, and the importance of magnetostriction in magnetite, *Earth Planet. Sci. Lett.*, *102*, 71-78, 1991.

Xu, S., and D. J. Dunlop, Micromagnetic modeling of Bloch walls with Néel caps in magnetite, *Geophys. Res. Lett.*, *23*, 2819-2822, 1996.

Xu, S., and R. T. Merrill, Microstress and coercivity in multidomain grains, *J. Geophys. Res.*, *94*, 10,627-10,636, 1989.

Xu, S., and R. T. Merrill, Microcoercivity, bulk coercivity and saturation remanence in multidomain materials, *J. Geophys. Res.*, *95*, 7083-7090, 1990.

Xu, S., and R. T. Merrill, Stress, grain size and magnetic stability of magnetite, *J. Geophys. Res.*, *97*, 4321-4329, 1992.

D. J. Dunlop and Ö. Özdemir, Department of Physics, Erindale College, University of Toronto, 3359 Mississauga Road North, Mississauga, Ontario, Canada L5L 1C6. (e-mail: dunlop@physics.utoronto.ca; ozdemir@physics.utoronto.ca)

(Received November 21, 1996; revised June 7, 1997;
accepted June 13, 1997.)